ANNUAL REVIEWS

Annual Review of Analytical Chemistry

Laser Desorption Combined with Laser Postionization for Mass Spectrometry

Luke Hanley, Raveendra Wickramasinghe, and Yeni P. Yung

Department of Chemistry, University of Illinois at Chicago, Chicago, Illinois 60607, USA; email: lhanley@uic.edu

Annu. Rev. Anal. Chem. 2019. 12:225–45

First published as a Review in Advance on February 20, 2019

The *Annual Review of Analytical Chemistry* is online at anchem.annualreviews.org

https://doi.org/10.1146/annurev-anchem-061318-115447

Keywords

laser ablation, laser desorption, postionization, mass spectrometry, imaging, photoionization

Abstract

Lasers with pulse lengths from nanoseconds to femtoseconds and wavelengths from the mid-infrared to extreme ultraviolet (UV) have been used for desorption or ablation in mass spectrometry. Such laser sampling can often benefit from the addition of a second laser for postionization of neutrals. The advantages offered by laser postionization include the ability to forego matrix application, high lateral resolution, decoupling of ionization from desorption, improved analysis of electrically insulating samples, and potential for high sensitivity and depth profiling while minimizing differential detection. A description of postionization by vacuum UV radiation is followed by a consideration of multiphoton, short pulse, and other postionization strategies. The impacts of laser pulse length and wavelength are considered for laser desorption or laser ablation at low pressures. Atomic and molecular analysis via direct laser desorption/ionization using near-infrared ultrashort pulses is described. Finally, the postionization of clusters, the role of gaseous collisions, sampling at ambient pressure, atmospheric pressure photoionization, and the addition of UV postionization to MALDI are considered.

1. INTRODUCTION: CAN MALDI BE IMPROVED WITH POSTIONIZATION?

MS: mass spectrometry

MALDI: matrix-assisted laser desorption/ionization performed with ultraviolet nanosecond laser desorption

LDPI-MS: laser desorption postionization MS; fs or ns refers to desorption laser pulse length of separate laser for postionization by various wavelength pulses

SPI: single-photon ionization, performed here with vacuum or extreme ultraviolet radiation

VUV: vacuum ultraviolet, typically 7.5 eV to ~13 eV of photon energy

Pulsed lasers have been widely utilized for sampling of molecular analytes in mass spectrometry (MS), leading to several prior reviews in this journal (1–4). Laser sampling can be most simply characterized as occurring via either a gentle desorption of intact neutral molecules or an ablation that is more of an explosive ejection of material, part of which might be charged. Since its introduction over three decades ago (5, 6), matrix-assisted laser desorption/ionization (MALDI) has become the most widely used method in laser sampling MS and is particularly dominant in MS imaging (7–10), where it is used by ~95% of all laboratories (11). The widespread adoption of MALDI has been facilitated by methodological reports for many applications (7–9, 12, 13). There are also several closely related strategies in laser desorption/ionization that can be implemented on MALDI platforms (14–16). Recent reviews have summarized MALDI quantification strategies (17) and the several competing theories on its opaque ion formation mechanism (2–4).

Nevertheless, there are ongoing limitations to MALDI that have birthed competing strategies in laser desorption. MALDI's desorption and ionization events are coupled in a multistep process (2–4), but most of the material desorbed from a sample is neutral and therefore not detectable in MS (7, 9). MALDI also suffers from differential ion efficiency and ion suppression that complicate and limit many analyses, especially applications involving imaging (18) and/or quantification (17). There is a vast literature describing the wide array of matrix compounds and strategies for their application, including crystallization conditions as well as sample treatments such as desalting and washing (7–9, 12, 13, 17). However, following these literature recipes can be a barrier to successful analyses as they can be sample dependent, time consuming, expensive, and/or difficult. Finally, sample charging in MALDI can limit mass accuracy and mass resolution as well as lateral resolution in MS imaging experiments.

These and other limitations of MALDI have led to the implementation of lasers beyond the ultraviolet (UV) nanosecond (ns) pulsed lasers that are most common in MALDI. Laser sampling has been demonstrated with ns to femtosecond (fs) pulsed lasers across a wide range of wavelengths (19–23). Postionization has been coupled to nearly all of these different varieties of laser sampling (19–22, 24–26). Postionization of neutral species in the gas phase occurs separately in space and time from the target from which those neutrals were volatilized in a prior desorption or ablation event. The separation of ionization from desorption/ablation can improve sensitivity and quantification, can reduce electrical charging effects, and is more amenable to modeling.

This review focuses primarily on one pathway to move laser sampling beyond MALDI: molecular analysis by laser desorption postionization mass spectrometry (LDPI-MS), also known as two-laser MS, as shown schematically in **Figure 1** (20, 21, 24, 25, 27). A description of single-photon ionization (SPI) by vacuum ultraviolet (VUV) radiation is followed by a brief consideration of multiphoton, short pulse, and other postionization strategies. This review focuses on postionization with pulsed lasers, but some comparisons are made with postionization using VUV synchrotron radiation, VUV lamps, and electrospray. Much of what is covered in this review is also applicable to the combination of laser postionization with the ion sputtering employed in secondary ion mass spectrometry, one focus of a separate review in this volume (28). The impacts of laser pulse length and wavelength are considered for sampling at low pressure, with an additional focus on atomic and molecular analysis by direct laser desorption/ionization using ultrashort pulses of near-infrared (IR) radiation. Discussion of postionization of clusters, the role of gaseous collisions, sampling at ambient pressure (19, 22, 23, 29, 30), atmospheric pressure photoionization (31), and the addition of UV postionization to MALDI (26) leads to concluding comments regarding future research directions.

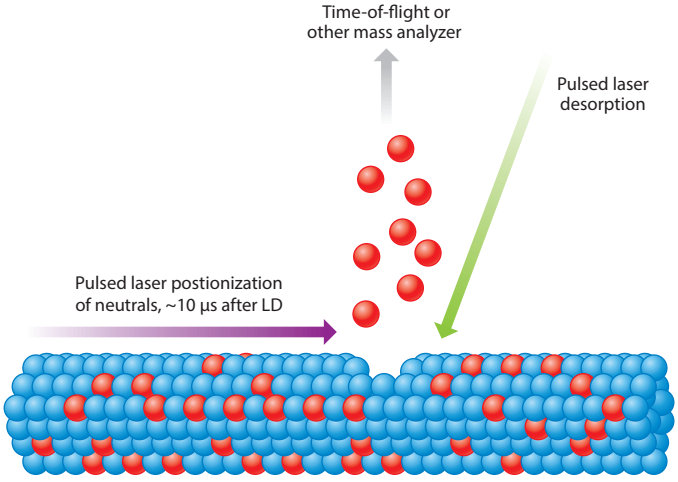

Figure 1

Schematic of laser desorption photoionization mass spectrometry (LDPI-MS). A pulsed laser (*green*) is focused onto the sample plate to volatilize analyte via desorption or ablation: Nanosecond (ns), picosecond (ps), and femtosecond (fs) laser pulses of various wavelengths have been used for this purpose. A pulsed laser beam (*purple*) is used for postionization of the resultant neutral plume, implemented using a wide range of pulse lengths and wavelengths.

2. LASER-BASED POSTIONIZATION

A primary goal of this review is to show the capabilities of detecting intact molecular species when VUV postionization is coupled to laser sampling for the enhanced detection of molecular neutrals. VUV postionization at low pressure is traditionally thought to proceed via SPI, which is especially effective when the photon energy used for ionization is only a few electron volts above the ionization energy of the target analyte (24, 32–34). The yield of ions, Y, formed by SPI of neutrals, can be described by $Y = \sigma_{spi} I N_{gas}$, where σ_{spi} is the photoionization cross section, I is the intensity of VUV radiation, and N_{gas} is the density of gaseous neutrals (24). SPI's linear dependence of ion yield on laser intensity is particularly attractive for quantification. The range of known cross sections, branching between SPI and photodissociation to neutrals, as well as other fundamental aspects were discussed previously (24).

Several studies have indicated that the optimum trade-off between maximum cross section and minimal fragmentation for SPI often occurs near ~10-eV photon energy (24, 32, 33, 35). The ninth harmonic of an ns pulsed Nd:YAG laser at 10.5 eV (118 nm) is therefore well suited to general SPI, allowing for low fragmentation of many molecular analytes while excluding ionization of water, carbon dioxide, nitrogen, hydrogen, and other common but uninteresting background gases (33, 36). However, this 10.5-eV laser source suffers from very low laser fluences (<1 μJ/pulse) and low pulse repetition rates of 10–200 Hz that slow the collection of MS images.

Several other sources of pulsed VUV radiation are available, but they differ considerably in photon energy, fluence, and repetition rate. The fluorine excimer laser is experimentally the most convenient and accessible ns pulsed VUV source, generating >1-mJ pulses at up to 1 kHz repetition rates. However, the fluorine excimer laser outputs 7.9 eV (157.6 nm) radiation that only allows SPI of species with relatively low ionization energies such as polyaromatic hydrocarbons (24), other extensively conjugated molecular systems, and certain pharmaceutical compounds (37, 38). A pulsed extreme UV gas discharge laser that outputs microjoule pulses at 46.9 nm

(26.4 eV) at <10-Hz repetition rates (39) can also be used for SPI of essentially any molecular species (40), but the higher photon energy can lead to considerably more fragmentation compared to VUV SPI (41). There are also tunable sources of VUV radiation: beamlines at synchrotron light sources (42–45) as well as laboratory-based tunable laser systems (46, 47), though the need for a VUV-emitting synchrotron for the former and the experimental complexity of the latter have limited their application for analysis.

ns-LD: nanosecond laser desorption using ~1–10-ns pulses of usually ultraviolet (but sometimes near-infrared) radiation

LITD: laser-induced thermal desorption

3. NANOSECOND LASER DESORPTION POSTIONIZATION

Nanosecond laser desorption postionization-MS (ns-LDPI-MS) has most commonly been performed with UV nanosecond-laser desorption (ns-LD) that allows spatial resolution of a few microns in imaging mode (45). High-quality optics such as a Schwarzschild microscope permit focusing of the desorption laser to near one micron, approaching the diffraction limit (27, 48). However, signal loss in the mass analyzer as well as the mechanism of desorption can degrade lateral resolution from the focused laser spot. The mechanism and efficiency of desorption/ablation and ionization depend upon the wavelength, fluence, and pulse length of the laser radiation; the optical properties of the solid target; and the timescale/energy of the laser-solid interaction (16, 49, 50). Also critical in this regard is the presence in the sample of a matrix, nanostructure, or other chromophore, as these permit the laser radiation to be resonantly absorbed, either electronically or vibrationally. For example, UV ns laser pulses induce a linear optical absorption within the matrix in MALDI, followed by an explosive ablation of a range of particulates that results in ion formation through a complex process, the detailed steps of which are still under debate (2–4). UV ns-LD of molecular species from porous silicon oxide and other nanostructures also occurs resonantly, dramatically increasing efficiency (15, 16). Regardless of wavelength, whether or not ns-LD is resonant with some component of the target will have a large impact on the desorption efficiency.

Ns-LD can follow a variety of mechanisms in the absence of resonant absorption but permits direct formation of useful molecular ion signal in only limited cases. Ns-LD of molecules on a flat metal or semiconductor surface is often explained by laser-induced thermal desorption (LITD). Early work showed that heat transfer following the resonant absorption of UV or near-IR ns pulsed laser radiation by the substrate leads to surface temperature changes that closely followed the laser pulse time profile (27, 51, 52). It was argued that the rapid heating rate in LITD can kinetically enhance intact molecular desorption while suppressing the thermal decomposition that can dominate at slower (i.e., resistive) heating rates (27). Analysis of experimental velocity distributions of various laser desorbed neutral molecules indicated translational temperatures of 300–400 K, in support of LITD followed by cooling via gas-phase collisions in the desorption plume (45). Supersonic jet cooling of molecules formed by ns-LD also reduces their fragmentation upon SPI due to their lower initial internal energy (see below) (53) and has permitted SPI of kilodalton-sized species (54, 55). While LITD might be considered dominant in only limited types of samples, more recent simulations support the LITD mechanism for molecular desorption from semiconductor surfaces (56), metal oxide nanoparticles, and colloidal graphite (57).

Postionization is an effective strategy to generate or enhance ion signal for both thermal and nonthermal mechanisms of laser desorption. For example, postionization strategies appear essential to detect the entirely neutral flux of molecular species generated by laser-induced acoustic desorption (58, 59) as well as ns or picosecond (ps) laser ablation by mid-IR radiation (19, 22, 23). Signal from MALDI has also been dramatically enhanced by UV laser postionization (26, 60) (see below).

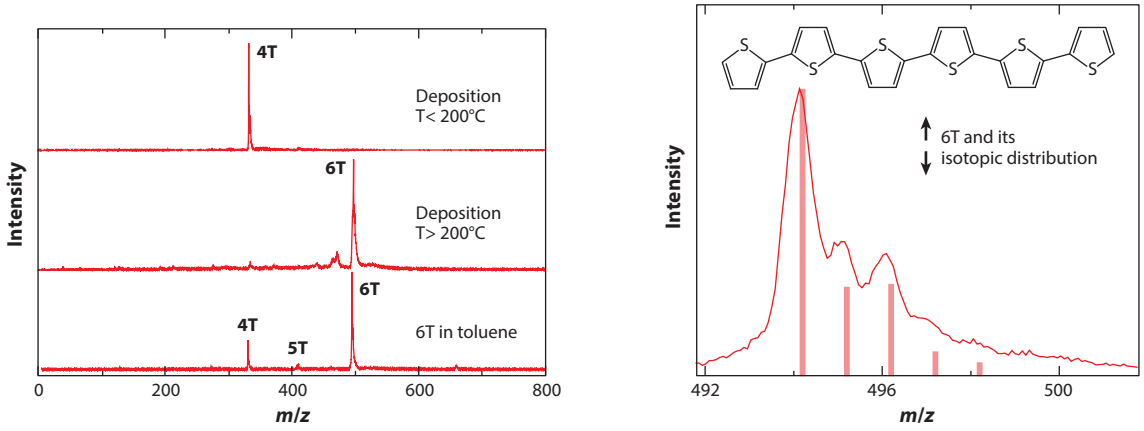

Figure 2

Nanosecond laser desorption photoionization (ns-LDPI) mass spectrum recorded with 7.9-eV postionization of various films nominally composed of sexithiophene (6T). The bottom left spectrum shows quaterthiophene (4T) and other impurities in addition to 6T. The middle left and upper left spectra demonstrate zone sublimation purification of 6T and 4T from the same sample, respectively. At right is the isotopic distribution of 6T (*red bars*; structure at top) overlaid on the actual 7.9-eV ns-LDPI mass spectrum.

A recent overview of LDPI-MS reviewed experimental strategies and demonstrated ns-LDPI-MS imaging of an electrically insulating sample (25). A variety of sample types have been analyzed by ns-LDPI-MS, including bacterial biofilms (24, 38), polymeric multilayers (34), nanocomposite films (62), and photoresists (45). Ns-LDPI-MS has also been used to characterize pharmaceutical drug compounds (63), asphaltenes in complex petroleum mixtures (64–66), dye and folic acid in tissue (67, 68), and ink on paper (69). A few examples of ns-LDPI-MS are expanded upon below, followed by some comments on short pulse postionization strategies.

3.1. Analysis of Organic Films for Electronic Devices by Ns-LDPI-MS

Films of conductive and semiconductive organic oligomers such as the oligothiophenes have been long examined for use in photovoltaics, light-emitting diodes, and other electronic devices (70). An example of the ability of ns-LDPI-MS to detect intact molecule species in such films is shown on the left side **Figure 2**, where all spectra were recorded using the 7.9-eV laser to postionize species desorbed by 349 nm, ~5-ns laser pulses (62). The bottom (left) spectrum is that of a commercially obtained sample of sexithiophene (6T, whose structure is shown in the inset on the right) prepared by dissolution in toluene, then dried onto a substrate. This solution-prepared sample (labeled 6T in toluene) displays a large quaterthiophene (4T) impurity with lesser amounts of other oligothiophenes (5T and 8T). The middle and top 7.9-eV ns-LDPI mass spectrum showed that zone sublimation could prepare pure films of 6T or 4T from the commercial sample by controlling the deposition temperature. Furthermore, the 7.9-eV ns-LDPI mass spectrum preserved the isotopic distribution of 6T (see spectrum at right, with solid vertical bars indicating theoretical isotopic distribution), facilitating peak identification due to the 4% natural abundance of ^{34}S and the 1% abundance of ^{13}C. Fragmentation, protonation, and/or deprotonation during many other desorption/ionization strategies might not have permitted identification of these different oligothiophenes or such a determination of their isotopic distribution. The 7.9-eV ns-LDPI mass spectrum was also able to provide evidence for the chemical binding of 4T to semiconductor nanoparticles in nanocomposite films (data not shown in the figure).

3.2. Quantification of Antibiotic in a Film by Ns-LDPI-MS

PCA: principal component analysis, commonly used for automated analysis of MS data

The growth of bacterial or fungal biofilms on medical device surfaces can lead to serious adverse health consequences (71). The slow release of antibiotic from a medical device is one established method for inhibiting biofilm growth (72), and ns-LDPI-MS was shown capable of detecting antibiotics within biofilms (35). A strategy for quantifying the release of an antibiotic from a porous substrate into a biofilm was then developed using 7.9-eV ns-LDPI-MS (38). Varying amounts of an antibiotic, a modified version of ampicillin, were adsorbed onto polyelectrolyte multilayers on gold substrates, which were then sterilized. *Enterococcus faecalis* biofilms were grown on thick polymer membranes, then inverted onto the antibiotic-doped multilayers and incubated for 18 h. The antibiotic leached from the multilayer and into the biofilm during this period, inhibiting biofilm growth. The amount of antibiotic in the multilayers before and after exposure to the biofilm was then quantified by 7.9-eV ns-LDPI-MS using a standard addition method, determining the amount of antibiotic needed to inhibit biofilm growth.

3.3. Distinguishing Genetically Similar Biofilms

Ns-LDPI-MS was also used to distinguish genetically similar strains of *Escherichia coli* biofilms (73). 7.9 eV ns-LDPI-MS was used to analyze metabolites from cocultured biofilms of two strains of *E. coli* (referred to as tomato and citrine), which differed from the wild-type K-12 strain by approximately four gene deletions each. The coculture biofilms were prepared by inoculating each pure strain a few millimeters apart on the same porous polycarbonate membrane, then letting the resultant colonies grow toward each other until they overlapped. **Figure 3*a*** represents the principal component analysis (PCA) of 7.9-eV ns-LDPI-MS data on the cocultured biofilm. PCA grouped the MS data into three distinct regions: the two monocultures and their overlapping area. Metabolic interactions within the overlapped region appeared to render it physiologically distinct from the pure regions. **Figure 3*b*** is a scree plot showing the variance of the complete

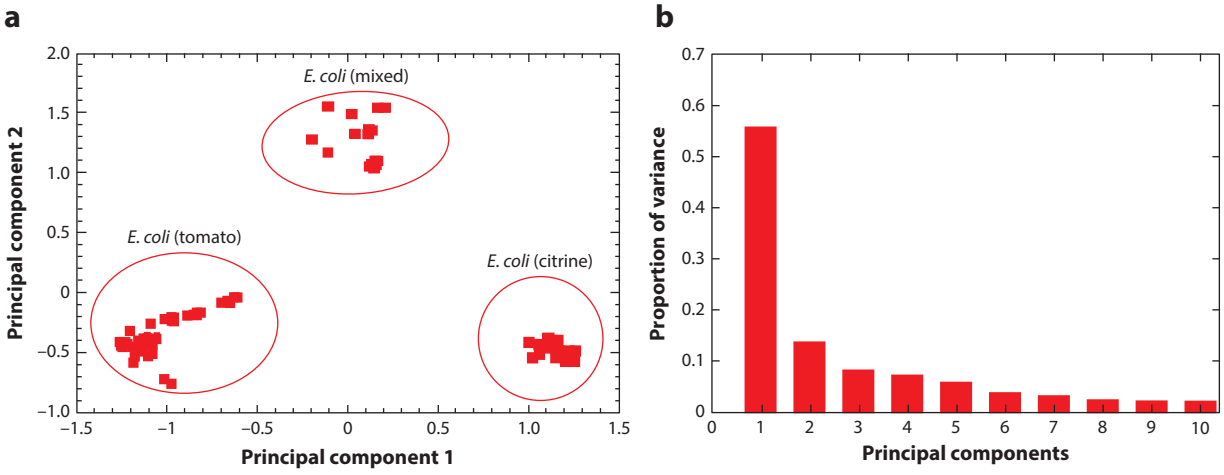

Figure 3

(*a*) Principal component analysis of 7.9-eV nanosecond laser desorption photoionization mass spectrometry (ns-LDPI-MS) of the three different regions of a coculture multistrain *Escherichia coli* (tomato and citrine strains) membrane biofilm. (*b*) Scree plot showing variance of the entire data set with respect to the principal components. Adapted with permission of the corresponding author from Reference 73, published by the Royal Society of Chemistry.

data set versus principal components, indicating that ~75% of the data is represented by the first two principal components. PCA of 7.9-eV ns-LDPI-MS data of pure regions showed a greater variance in the second principal component compared to similar measurements by 10.5-eV ns-LDPI-MS (data not shown). The observed difference in PCA spreads can be explained by the fact that many compounds have ionization energies between 9 and 10 eV, so 7.9-eV SPI samples a subset of molecules with lower ionization energies, whereas 10.5-eV SPI detects a wider range of analytes.

REMPI: resonance-enhanced multiphoton ionization, usually performed using nanosecond ultraviolet pulses

LAESI: laser ablation electrospray ionization using ~10-ns mid-infrared (~3,000 nm) pulses

3.4. Multiphoton and Short Pulse Postionization in Ns-LDPI-MS

Single-photon ionization was used in the aforementioned examples, but resonance-enhanced multiphoton ionization (REMPI) can also be utilized in ns-LDPI-MS (25). REMPI has much higher selectivity than simply tuning the photon energy in SPI (74, 75). Applications and the various advantages of REMPI, including its capability to distinguish chiral isomers, have been discussed previously in this journal (76, 77). For example, two-photon REMPI can be accessed in many molecules via the fourth or fifth harmonic of a pulsed Nd:YAG laser or a tunable optical parametric oscillator equipped with second or third harmonic generation. Two examples of ns-LDPI-MS with REMPI are an organic analysis for planetary missions (78) and a fundamental study of the laser ablation of ice (79).

Molecular fragmentation can be excessive for many molecular species with REMPI using ns laser pulses (74, 75), but shortening the pulse length can reduce molecular fragmentation (75). The development of chirped pulse amplification has made fs laser pulses available for both postionization and also laser ablation, as discussed further below (80). An example of the use of ultrashort laser pulses (<100 fs) for postionization in ns-LDPI-MS is shown in **Figure 4**, where the artificial amino acid 2,5-dibromotyrosine was analyzed using 349-nm ns-LD and 267-nm, ~75-fs laser postionization at various fluences and fixed delay time (81). **Figure 4*a*** displays the precursor structure (M) as well as those of the observed fragments, in clockwise order of descending mass (I–VI). **Figure 4*b*** shows that overall signal increased with fluence, while **Figure 4*c*** shows that the precursor ion (M^+) was a relatively minor component with extensive fragmentation that mostly stabilized at an intermediate fluence. However, analysis of this amino acid by 10.5-eV ns-LDPI-MS (not shown) displayed slightly less fragmentation.

The results shown in **Figure 4** are consistent with experiments performed two decades ago that essentially differed only in the amino acids analyzed and the use of thermal evaporation in lieu of ns-LD (82, 83). Recent studies have found that using yet shorter (<50-fs) UV laser pulses for ionization of gaseous species further reduces fragmentation (84). When considered along with other recent work that has combined ion sputtering with postionization by near-IR ultrashort pulses (28, 85, 86), it is clear that ultrashort pulse postionization holds great promise for application to LDPI-MS, secondary neutral MS, and beyond.

4. SHORT PULSE LASER ABLATION AND FS-LDI-MS

As is the case with postionization, shortening the laser pulse length below the nanosecond regime can access new phenomena that are highly advantageous for MS sampling. Laser pulses in the mid-IR (~3,000 nm) are resonant with OH vibrations in water, effectively ablate water-containing samples (87), and form the basis of laser ablation electrospray ionization (LAESI) (22, 88). However, it has been argued that shortening the mid-IR ns laser pulse lengths down to 10–100 ps increases the coupling of excited OH vibrations into the translational motion required for ablation while reducing energy transfer into the sample (89). This reduction in the transfer of thermal and

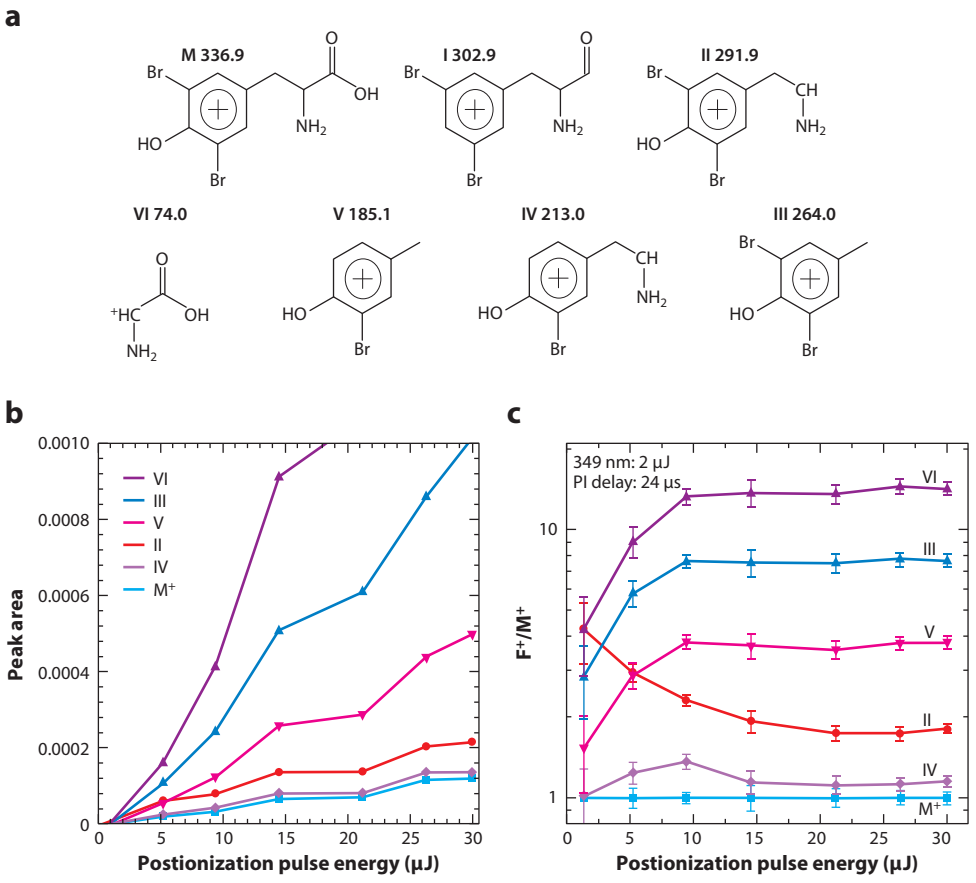

Figure 4

(*a*) Structure of 2,5-dibromotyrosine precursor ion (M^+) and fragments (I–VI) observed by nanosecond laser desorption photoionization mass spectrometry (ns-LDPI-MS) using 267-nm, ~75-fs laser postionization. (*b*) Intensity of M^+ and fragments versus postionization laser pulse energy. (*c*) Fragment/precursor ion ratios versus postionization laser pulse energy. Adapted with permission of the author from Reference 81.

acoustic energy can explain an observed reduction in sample damage and molecular fragmentation with ps laser pulses. The overall process is referred to as picosecond infrared laser desorption via impulsive vibrational excitation (PIRL-DIVE), an effective strategy for laser surgery (90) and ablation for MS both without (91) and especially with (23) postionization.

PIRL-DIVE: 10–100-picosecond infrared laser desorption via impulsive vibrational excitation

fs-LA: femtosecond laser ablation by 50–100-fs near-infrared (800–1,100-nm) pulses

PIRL-DIVE is apparently driven by a vibrationally resonant excitation that does not lead to photoionization (89), but electronic excitation that does lead to photoionization and then ablation can be accessed nonresonantly via even shorter, <100-fs laser pulses. In fact, such ultrashort pulses of even near-IR radiation can ablate virtually any material when focused to fluences of 10^{12} to 10^{15} W/cm^2 (92–94). Excitation by <100-fs laser ablation (fs-LA) commences with a highly nonlinear optical absorption, leading to either nonresonant multiphoton ionization or tunneling ionization that causes electron temperatures in a sample to increase before lattice motion, reducing sample damage (56). Relaxation of this electronic excitation into the resultant plasma induces melting, evaporation, shock waves, and/or bubble formation within the sample, which can then lead to an ablative ejection of neutral and ionized atoms, molecules, clusters, and particulates.

Fs-LA of water has been described in detail (95) and is summarized here as an example. The exposure of water to fs laser fluences near the ablation threshold initially induces nonlinear photoionization, avalanche ionization, and photodissociation that generate secondary electrons, radicals, atoms, and other neutrals that collectively form a highly localized plasma. The subsequent <100-ps local heating by the plasma results in the formation of short-lived bubbles whose small size and transient nature, combined with the moderate temperature increase associated with their formation, localize the ablation event compared with ns laser excitation. Finally, ejection of condensed-phase material into the gas phase occurs, releasing the stress confinement in these bubbles. Similar processes have been proposed for fs-LA of polymer and organic systems that are also thought to be distinct from those induced by ns laser pulses (96).

fs-LDI: direct (single) femtosecond laser desorption/ionization by 50–100-fs near-infrared (800-nm) pulses

Relatively low thermal damage and a highly confined ablation event allow fs-LA to more precisely cut both opaque and transparent materials when compared to longer laser pulses. Metals, glasses, silicon, and other materials (94) have all been micromachined by fs-LA with submicron spatial accuracy, leaving behind smooth and relatively undamaged surfaces. Mammalian tissue (93) and other cellular structures (97, 98) can also be cut cleanly by fs-LA, a phenomenon long exploited for laser surgery (93). For example, tissue excision by fs-LA at repetition rates of $\leq$1 kHz produces very clean cuts compared to ns pulse lengths (95).

These attractive characteristics have also led to the use of fs-LA for sampling of dielectric, conductive, and semiconductive materials for MS analysis, without the need for added matrix or another chromophore while overcoming the sample-dependent fluctuations in desorption efficiency of optically resonant versus nonresonant ns-LD (20–22, 99, 100). Experiments tested the capability of ~75-fs, 800-nm fs-LA to cut bovine eye tissue with high precision (101). MALDI-MS was then used to compare phospholipids and <6-kDa peptides that were lysed from proteins on native bovine eye tissue and fs-LA modified tissue: Both showed similar mass spectra, indicating that fs-LA can be performed in a fashion that causes relatively little chemical damage to the remaining tissue (101). This and prior results on bacterial biofilms were used to argue for the potential of fs-LA for depth profiling (20, 101, 102).

Unlike the intact sample surface left behind after fs-LA, the fate of the ablated material that is ejected into the gas phase is an altogether different story. The ratio of ejected ions to neutrals and the extent of molecular fragmentation from a given sample depend upon the laser fluence and shielding of the sample by the laser-induced plasma (92). Fs-LA is used for a sampling feed into inductively coupled plasma MS for elemental analysis (92).

However, atomic ions are formed directly in fs-LA under the appropriate laser conditions (99, 103) and allow ~800-nm, <100-fs laser pulses to be used for direct fs-laser desorption/ionization (fs-LDI) (99, 103–105). There is a fluctuation in sensitivity for different elements detected by fs-LDI-MS that limits its application compared to fs-LA-inductively coupled plasma MS (103, 104). Nevertheless, the impressive depth and spatial resolution for fs-LDI-MS as well as its experimental simplicity have provided this relatively new strategy with a growing niche for elemental analysis (99, 105–107).

The detection of molecular species by fs-LDI-MS has also been examined, and an excellent test case is the detection of lipids within tissue, a common application of MALDI-MS imaging (7–9, 108). The detection of lipids with fs-LDI-MS was combined with multivariate analysis to map lipids within human pancreatic tissue samples (109). Approximately 10-μm-thick tissue slices were mounted on indium tin oxide–coated glass slides, submerged in lithium chloride/formalin to enhance the formation of lithiated ions (108), dried, evacuated, then analyzed by fs-LDI-MS. **Figure 5*b*** shows the total ion image from fs-LDI-MS of tissue as well as the result of maximum a posteriori analysis of the collected fs-LDI-MS data, which were grouped into two categories

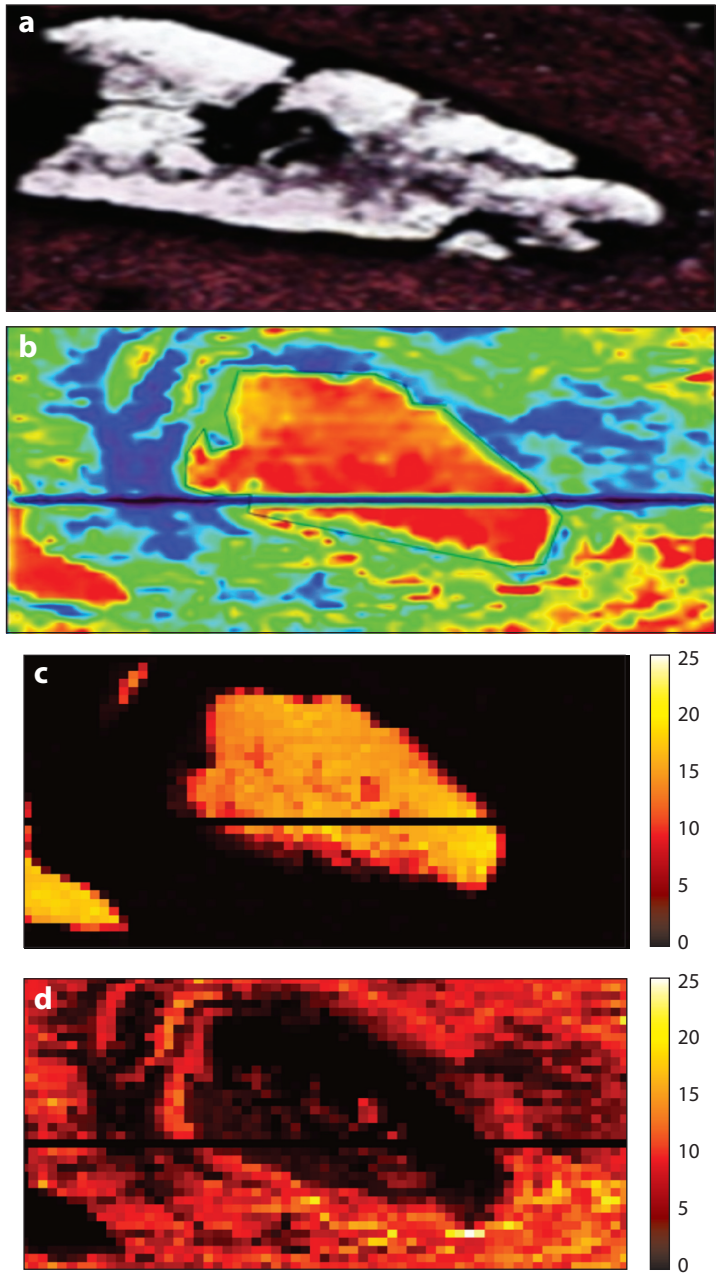

Figure 5

(*a*) Optical image of pancreas tissue slice that has been H&E stained to show adipocytes (fatty tissue). (*b*) Total ion image from femtosecond laser desorption/ionization mass spectrometry (fs-LDI-MS) of adjacent tissue slice. (*c*) Lipid and (*d*) nonlipid components extracted by multivariate analysis of the fs-LDI-MS data. Analysis area: 630 × 360 μm^2. Note that the upper two images are elongated slightly. Ion intensities are shown using a heat scale. Adapted from Reference 109, with the permission of the American Vacuum Society.

that were identified as (**Figure 5*c***) lipid and (**Figure 5*d***) nonlipid regions by correlation with (**Figure 5*a***) bright field transmission optical microscopy of stained samples.

The shortcoming of fs-LDI-MS, for at least this lipid analysis on this particular mass analyzer, is that the observed ions (109) differ from the intact precursor (parent) ions of phosphatidylcholine or other lipids observed by MALDI-MS (8, 108). Rather, the lipid-related ions detected by fs-LDI-MS appeared to be atypical fragments that were not identified in this study. Excessive molecular fragmentation is also a concern with LDI-MS using vacuum or extreme UV ns laser pulses (110, 111), although both display high potential for submicron spatial resolution for MS imaging (112, 113), and depth profiling has been demonstrated with at least the latter (113).

RRKM: Rice-Ramsperger-Kassel-Marcus theory describing the unimolecular dissociation of ions

5. FS-LDPI-MS, PLUME EXPANSION, AND THE EFFECT OF DELAY TIME BETWEEN LASERS

The most promising approach for using fs-LA for MS analysis is to couple it to postionization. Fs-LDPI-MS coupled with 10.5-eV postionization was used to detect various intact small molecular species in tissue (100), in biofilms (20), and from test patterns (21). Multiphoton (76, 77) and short pulse ionization methods (81–85) can also be coupled with fs-LA at low pressures for molecular analysis (see above). Prior work has discussed coupling fs-LA at ambient pressure with electrospray postionization (22), and discharge-based postionization is also possible (30). More thorough comparison of all the postionization methods is warranted, although it should be noted that the relatively long durations of electrospray plumes and discharges are not optimal for coupling to the temporally compressed ablation plume formed by fs-LA (or ns-LD).

The question arises as to whether fs-LA is excessively energetic for sampling in molecular MS, especially given the aforementioned observation of atomic ions by fs-LDI-MS. The accepted model for fragmentation of molecular ions in mass spectrometry is that it occurs unimolecularly and is controlled by the internal energy imparted by the volatization/ionization event(s) to the precursor (parent or molecular) ion in the gas phase (114). Internal energy can derive from the desorption event (32), hence the fragmentation reduction upon cooling (53–55), or the ionization event. Rice-Ramsperger-Kassel-Marcus (RRKM) theory has been used generally to estimate the internal energies of thermometer ions (114) and applied specifically to interpret the fragmentation of benzyl pyridinium thermometer ions formed by various laser-based strategies via correlation with calculated unimolecular rate constants (115). Thermometer ions desorbed at low pressures by MALDI via UV ns pulses with α-cyano-4-hydroxycinnamic acid matrix were thereby estimated to impart ~3.7 eV of internal energy (115, 116), compared with ~4.3 eV by fs-LDI-MS (100) and ~4.1 eV by 10.5-eV fs-LDPI-MS (100). These studies indicated that fs-LDPI-MS can produce precursor ions that are only slightly more energetic than those generated by traditional MALDI. A more quantitative comparison of these methods is probably not warranted given differences in the data analysis methods and/or other experimental parameters (100).

Fragmentation can clearly be tuned by variation of the ablation laser fluence, where higher fs-LA fluences lead to enhanced molecular fragmentation (21, 100). Another strategy to increase the detection of intact molecule species in both ns- and fs-LDPI is to maximize the time delay between desorption/ablation and postionization laser pulses, as species that desorb with lower velocities tend to have lower internal energy resulting from a higher number of gas-phase collisions (45). Shorter delay times will often lead to enhanced fragmentation and can be used for structural analysis. The role of collisional cooling was verified in fs-LDPI-MS by the decrease in energy transfer with the high collision number that occurs with longer delay times between ablation and postionization laser pulses (100). Of course, the maximum delay time is constrained by the requirement that the postionization pulse intersect with as much of the ablation plume as possible, as the latter continues to expand over time as it travels away from the surface.

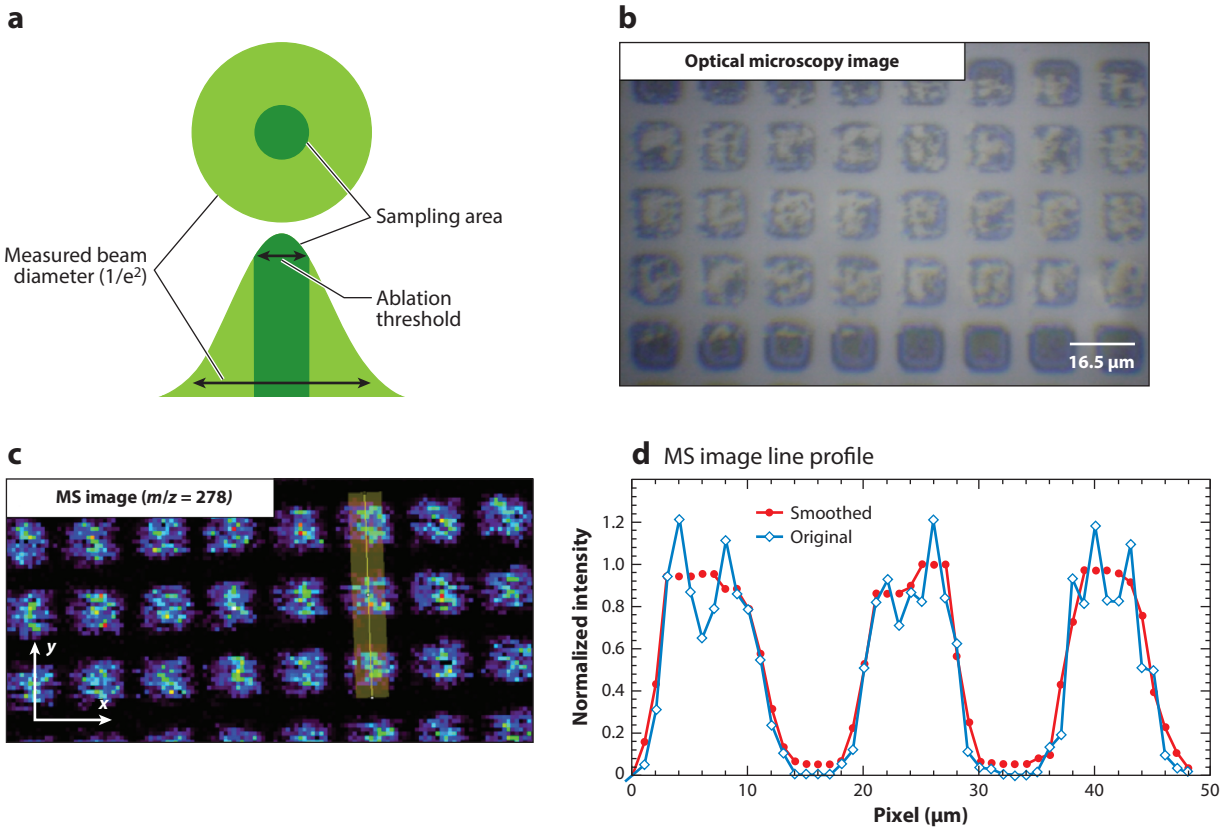

Figure 6

(*a*) Schematic of subdiameter imaging with femtosecond laser ablation (fs-LA) probe. Micrometer-scale square pattern of pentacene deposited onto an Si wafer by sublimation, imaged by (*b*) an integrated optical microscope after mass spectrometry (MS) analysis and (*c*) femtosecond laser desorption photoionization mass spectrometry (fs-LDPI-MS). Grid dimensions were: 16.5-µm pitch, 11.5-µm hole width, and 5-µm bar width. One MS image pixel corresponds to a 1-µm sample translation step. (*d*) The line scan for the MS image area demonstrates lateral resolution of ~2 µm, obtained by signal integration of the yellow shaded region in the MS image). Adapted from Reference 21, with the permission of the American Chemical Society.

Another advantage of fs-LDPI-MS is its demonstrated capability for high lateral resolution MS imaging that is shown in **Figure 6** (21). The additional signal afforded by fs-LDPI-MS compared to fs-LDI-MS allowed the former to sample an organic test pattern at lower laser fluences where ablation occurred from smaller volumes. An ~4-µm-diameter laser beam focal spot used for fs-LDPI-MS gave ~2-µm lateral resolution by exploiting the nonlinear optical absorption inherent to fs-LA, where only the intensity above a certain threshold leads to ablation (depicted schematically at the top of **Figure 6**) (21).

6. POSTIONIZATION OF CLUSTERS AND SAMPLING AT AMBIENT PRESSURE

VUV postionization of molecules at low pressures, where gas-phase collisions are largely absent, is traditionally thought to proceed by SPI leading to the ejection of a photoelectron and subsequent formation of a radical cation (24, 33) (see above). Nevertheless, such an initial SPI event

in a larger species like a cluster can be followed by loss of molecular fragments and formation of a smaller, protonated ion. Such events were observed, for example, in VUV postionization of acetaldehyde/water clusters forming protonated ions via loss of a deprotonated acetaldehyde neutral (117). Similar phenomena were observed in ns-LDPI-MS, where the lower ionization energies of clusters additionally allowed their detection at lower photon energies than expected based upon the ionization energies of their constituent molecules (34). SPI followed by dissociation of clusters is likely significant in many ns-LD and fs-LA events, given that abundant clusters are known to be generated in MALDI (2–4, 118) and other types of laser sampling (23, 89, 119). These phenomena must also be considered even though they complicate the traditional, gas-phase models of SPI, REMPI, and other types of laser postionization.

Like LDPI-MS, MALDI-MS is most commonly performed with samples at low pressures (7–9), allowing high sensitivity (120). Nevertheless, there are numerous advantages to laser sampling at elevated or even atmospheric pressure (ambient) (30, 91, 119, 121), some of which have already been discussed previously in this journal (22). Ambient sampling facilitates analysis of large and/or complex objects while precluding the dehydration of samples that occurs under vacuum. Among the many examples of ambient laser sampling for MS (30, 91, 119, 121), one of particular relevance to LDPI-MS involves its coupling to low-pressure VUV SPI-MS that was applied to explosives analysis (122).

Yet another advantage of ambient sampling in general is the internal cooling of ions that occurs as a result of the many gas-phase collisions during transmission from atmosphere to the evacuated mass analyzer. For example, significantly lower internal energies were observed for thermometer ions that were laser desorbed at ambient pressure: ~2.0 eV for both fs-LA (123) and mid-IR ns laser ablation (124), although both experiments employed electrospray rather than laser postionization. This is roughly half of the internal energy imparted by MALDI, fs-LDI, and fs-LDPI performed in vacuum (see above). Gas-phase collisions also help dissociate clusters and larger particles formed during laser desorption (4, 119), improving useful ion signal. However, it is unclear to what extent this offsets ion transmission losses from ambient sampling to the mass analyzer.

VUV postionization at ambient is known as atmospheric pressure photoionization (APPI) and is performed using noble gas discharges that emit an incoherent, continuous output of VUV radiation (31). One major difference from VUV postionization in vacuum is that in APPI, the VUV photons are strongly absorbed by air, perhaps before they can induce direct SPI of an analyte. Ionization in APPI is instead thought to proceed via a series of chemical ionization–like steps (31, 125), often via addition of a dopant that undergoes SPI, facilitates proton transfer to the analyte, and may also involve intermediate, protonated clusters. Similar proton and charge-transfer events initiated by VUV SPI are likely to occur via ion–molecule collisions within the high-density realm of ablation plumes, even for laser sampling at low pressures.

Several configurations of ambient laser sampling coupled to APPI have been reported: with mid-IR ns laser ablation APPI (LAAPPI) (126), near-IR ns-LD (127), and laser-induced acoustic desorption (128). Any of these configurations and the one shown in **Figure 7** permit facile coupling with the majority of modern high-resolution and tandem mass spectrometers that are built to be coupled with electrospray ionization. **Figure 7** depicts a recent iteration of ambient laser–based sampling coupled to APPI, a laser diode thermal desorption (LDTD) APPI (LDTD-APPI) source (129). The LDTD-APPI source combines a pseudocontinuous near-IR laser diode with a Kr discharge lamp and a dopant gas sprayer. This LDTD-APPI source gave similar mass spectra as mid-IR ns laser ablation (126) for *Salvia officinalis* (common sage) leaf with anisole dopant and a *Pseudomonas aeruginosa* biofilm with toluene dopant (129). The diode laser was a relatively inexpensive, battery-powered surgical laser, so the configuration could be implemented in portable MS.

APPI: atmospheric pressure photoionization, typically performed with continuous vacuum ultraviolet discharges

LAAPPI: mid-infrared nanosecond laser ablation atmospheric pressure photoionization using ~10-ns mid-infrared pulses

LDTD: laser diode thermal desorption performed using continuous near-infrared radiation (940 nm)

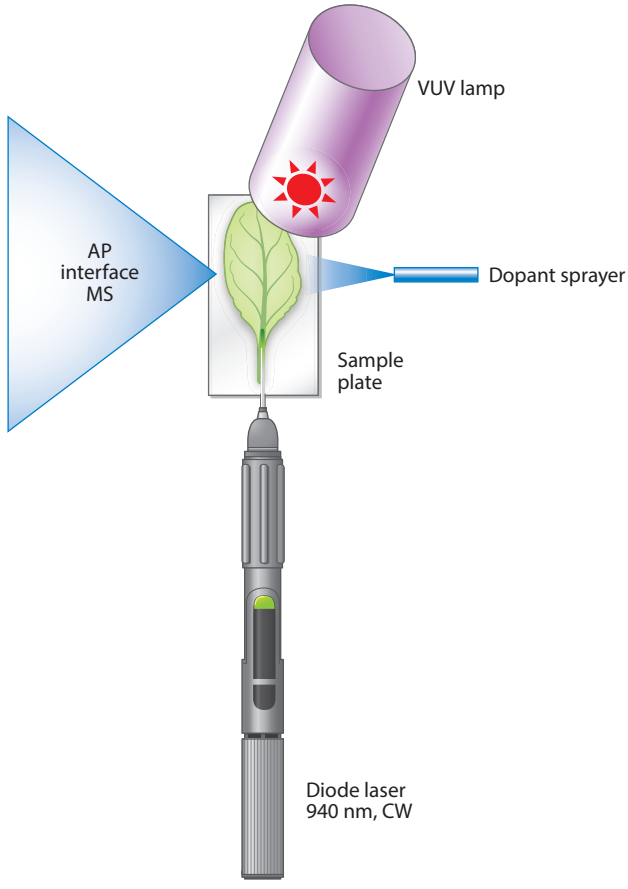

Figure 7

Schematic diagram of LDTD-APPI source. Adapted from Reference 129, with the permission of the American Chemical Society. Abbreviations: AP, atmospheric or ambient pressure; CW, continuous wave; LDTD-APPI, laser diode thermal desorption atmospheric pressure photoionization; MS, mass spectrometry; VUV, vacuum ultraviolet.

Because this review started with a discussion of MALDI, it is appropriate to again consider how this most popular method continues to evolve. Perhaps the oldest method of ambient laser–based sampling is atmospheric pressure MALDI (7, 9, 120, 130). A lateral resolution of 1.4-μm imaging has been demonstrated in atmospheric pressure MALDI using a Schwarzschild microscope configuration (131), although it is likely that insufficient signal will limit this resolution for many analyses. MALDI is also performed at intermediate pressure (9), to which UV postionization was coupled in a method termed MALDI-2 (26). MALDI-2 enhances ion signal by up to 100× for a variety of species from tissue. The postionization process of MALDI-2 was described as secondary MALDI on clusters and larger particulates that was observed to depend upon gas pressure as well as laser wavelength, delay, and pulse energy (see above). It was argued that MALDI-2 will lead to less fragmentation than photoionization, although the latter is also observed in MALDI-2 (26). Enhanced lipid imaging was also described for MALDI-2 in a configuration coupled to a high mass resolution mass spectrometer (60). Laser postionization has also been employed to probe clusters formed in MALDI (118, 132).

7. CONCLUSIONS

There are significant opportunities for analysis afforded by coupling laser postionization to laser desorption or ablation: the ability to forego matrix application, the high lateral resolution, improved analysis of electrically insulating samples, and an excellent potential for high sensitivity and depth profiling while minimizing differential detection. Nevertheless, the question must be asked: How might laser desorption postionization rise above MALDI and the plethora of other MS ion sources (15, 16, 22, 26, 29–31, 119, 121, 125) that continue to be described? First, commercial instrumentation must become available for users to develop protocols for specific applications of LDPI-MS. Second, these instruments will likely need to incorporate traditional chromatography, ion mobility, tandem MS, and/or high-resolution MS to compete in the realm of species identification with established methods. Third, commercialization may also require development of less expensive and more reliable postionization lasers, and such factors may ultimately dictate whether VUV ns, UV ns, or short pulse lasers come to dominate postionization in LDPI-MS and secondary neutral MS. Finally, bioinformatic strategies are needed for automated analysis of the large data sets that arise from LDPI-MS. Nevertheless, it is clear that the ongoing rapid development of new laser technologies will continue to open up new opportunities in laser-based MS, as it has already for the use of ultrashort laser pulses in LDPI-MS (20, 21, 81) and elsewhere (23, 133). Perhaps in another decade, the use of attosecond laser pulses will even come to be used in laser sampling MS (134).

DISCLOSURE STATEMENT

L.H. is currently funded by an analytical instrument company to explore commercial implementation of laser desorption postionization. The other authors are not aware of any affiliations, memberships, funding, or financial holdings that might be perceived as affecting the objectivity of this review.

ACKNOWLEDGMENTS

This work was supported by the National Institute of Biomedical Imaging and Bioengineering under grant 1U01EB019416. This material is based in part upon work supported while L.H. was serving at the National Science Foundation. L.H. thanks his many prior graduate students and colleagues including Melvin Blaze M.T., Chhavi Bhardwaj, Yang Cui, Jerome F. Moore, and Igor V. Veryovkin for their hard work, insightful discussions, and experimental contributions that made this work possible. The authors would also like to thank Cornelius Pieterse for his useful comments on the manuscript. Finally, L.H. has tried to focus the citations on relatively recent review articles and, as a result, apologizes to the community for not having been able to cite much foundational and important work in this area.

LITERATURE CITED

1. Burnum KE, Frappier SL, Caprioli RM. 2008. Matrix-assisted laser desorption/ionization imaging mass spectrometry for the investigation of proteins and peptides. *Annu. Rev. Anal. Chem.* 1:689–705
2. Bae YJ, Kim MS. 2015. A thermal mechanism of ion formation in MALDI. *Annu. Rev. Anal. Chem.* 8:41–60
3. Lu I-C, Lee C, Lee Y-T, Ni C-K. 2015. Ionization mechanism of matrix-assisted laser desorption/ionization. *Annu. Rev. Anal. Chem.* 8:21–39
4. Knochenmuss R. 2016. The coupled chemical and physical dynamics model of MALDI. *Annu. Rev. Anal. Chem.* 9:365–85

5. Tanaka K, Waki H, Ido Y, Akita S, Yoshida Y, Yoshida T. 1998. Protein and polymer analyses up to *m/z* 100 000 by laser ionization time-of-flight mass spectrometry. *Rapid Commun. Mass Spectrom.* 2:151–53
6. Karas M, Bachmann D, Bahr U, Hillenkamp F. 1987. Matrix-assisted ultraviolet laser desorption of non-volatile compounds. *Int. J. Mass Spectrom. Ion Process.* 78:53–68
7. Dreisewerd K. 2014. Recent methodological advances in MALDI mass spectrometry. *Anal. Bioanal. Chem.* 406:2261–78
8. Caprioli RM. 2014. Imaging mass spectrometry: molecular microscopy for enabling a new age of discovery. *Proteomics* 14:807–9
9. Spengler B. 2015. Mass spectrometry imaging of biomolecular information. *Anal. Chem.* 87:64–82
10. Murray KK, Seneviratne CA, Ghorai S. 2016. High resolution laser mass spectrometry bioimaging. *Methods* 104:118–26
11. Palmer A, Trede D, Alexandrov T. 2016. Where imaging mass spectrometry stands: here are the numbers. *Metabolomics* 12:107
12. Demirev PA, Fenselau C. 2008. Mass spectrometry for rapid characterization of microorganisms. *Annu. Rev. Anal. Chem.* 1:71–93
13. Buchberger A, Yu Q, Li L. 2015. Advances in mass spectrometric tools for probing neuropeptides. *Annu. Rev. Anal. Chem.* 8:485–509
14. Gurard-Levin ZA, Mrksich M. 2008. Combining self-assembled monolayers and mass spectrometry for applications in biochips. *Annu. Rev. Anal. Chem.* 1:767–800
15. Greving MP, Patti GJ, Siuzdak G. 2011. Nanostructure-initiator mass spectrometry metabolite analysis and imaging. *Anal. Chem.* 83:2–7
16. Stolee JA, Walker BN, Zorba V, Russo RE, Vertes A. 2012. Laser-nanostructure interactions for ion production. *Phys. Chem. Chem. Phys.* 14:8453–71
17. Rzagalinski I, Volmer DA. 2017. Quantification of low molecular weight compounds by MALDI imaging mass spectrometry—a tutorial review. *Biochim. Biophys. Acta Proteins Proteom.* 1865:726–39
18. Taylor AJ, Dexter A, Bunch J. 2018. Exploring ion suppression in mass spectrometry imaging of a heterogeneous tissue. *Anal. Chem.* 90:5637–45
19. Nemes P, Barton AA, Li Y, Vertes A. 2008. Ambient molecular imaging and depth profiling of live tissue by infrared laser ablation electrospray ionization mass spectrometry. *Anal. Chem.* 80:4575–82
20. Cui Y, Bhardwaj C, Milasinovic S, Carlson RP, Gordon RJ, Hanley L. 2013. Molecular imaging and depth profiling of biomaterials interfaces by femtosecond laser desorption postionization mass spectrometry. *ACS Appl. Mater. Interfaces* 5:9269–75
21. Cui Y, Veryovkin IV, Majeski MW, Cavazos DR, Hanley L. 2015. High lateral resolution versus molecular preservation in near-IR fs-laser desorption postionization mass spectrometry. *Anal. Chem.* 87:367–71
22. Flanigan P, Levis R. 2014. Ambient femtosecond laser vaporization and nanosecond laser desorption electrospray ionization mass spectrometry. *Annu. Rev. Anal. Chem.* 7:229–56
23. Zou J, Talbot F, Tata A, Ermini L, Franjic K, et al. 2015. Ambient mass spectrometry imaging with picosecond infrared laser ablation electrospray ionization (PIR-LAESI). *Anal. Chem.* 87:12071–79
24. Akhmetov A, Moore JF, Gasper GL, Koin PJ, Hanley L. 2010. Laser desorption postionization for imaging MS of biological material. *J. Mass Spectrom.* 45:137–45
25. Akhmetov A, Bhardwaj C, Hanley L. 2015. Laser desorption postionization mass spectrometry imaging of biological targets. In *Mass Spectrometry Imaging of Small Molecules*, Vol. 1203, ed. L He, pp. 185–94. New York: Springer Sci. Bus. Media
26. Soltwisch J, Kettling H, Vens-Cappell S, Wiegelmann M, Müthing J, Dreisewerd K. 2015. Mass spectrometry imaging with laser-induced postionization. *Science* 348:211–15
27. Hanley L, Kornienko O, Ada ET, Fuoco E, Trevor JL. 1999. Surface mass spectrometry of molecular species. *J. Mass Spectrom.* 34:705–23
28. Gilmore IS, Heiles S, Pieterse CL. 2019. Metabolic imaging at the single-cell scale: recent advances in mass spectrometry imaging. *Annu. Rev. Anal. Chem.* 12. In press. **https://doi.org/10.1146/annurev-anchem-061318-115516**
29. Huang M-Z, Yuan C-H, Cheng S-C, Cho Y-T, Shiea J. 2010. Ambient ionization mass spectrometry. *Annu. Rev. Anal. Chem.* 3:43–65

30. Cheng S-C, Shiea C, Huang Y-L, Wang C-H, Cho Y-T, Shiea J. 2017. Laser-based ambient mass spectrometry. *Anal. Methods* 9:4924–35
31. Kauppila TJ, Syage JA, Benter T. 2017. Recent developments in atmospheric pressure photoionization-mass spectrometry. *Mass Spectrom. Rev.* 36:423–49
32. Wilson KR, Jimenez-Cruz M, Nicolas C, Belau L, Leone SR, Ahmed M. 2006. Thermal vaporization of biological nanoparticles: fragment-free vacuum ultraviolet photoionization mass spectra of tryptophan, phenylalanine-glycine-glycine, and b-carotene. *J. Phys. Chem. A* 110:2106–13
33. Hanley L, Zimmermann R. 2009. Light and molecular ions: the emergence of vacuum UV single-photon ionization in MS. *Anal. Chem.* 81:4174–82
34. Blaze MTM, Takahashi LK, Zhou J, Ahmed M, Gasper GL, et al. 2011. Brominated tyrosine and polyelectrolyte multilayer analysis by laser desorption VUV postionization and secondary ion mass spectrometry. *Anal. Chem.* 83:4962–69
35. Gasper GL, Takahashi LK, Zhou J, Ahmed M, Moore JF, Hanley L. 2010. Laser desorption postionization mass spectrometry of antibiotic-treated bacterial biofilms using tunable vacuum ultraviolet radiation. *Anal. Chem.* 82:7472–78
36. Van Bramer SE, Johnston MV. 1990. 10.5 eV photoionization mass spectrometry of aliphatic compounds. *J. Am. Soc. Mass Spectrom.* 1:419–26
37. Finch JW, Toerne KA, Schram KH, Denton MB. 2005. Evaluation of a hydrogen laser vacuum ultraviolet source for photoionization mass spectrometry of pharmaceuticals. *Rapid Commun. Mass Spectrom.* 19:15–22
38. Blaze MTM, Akhmetov A, Aydin B, Edirisinghe PD, Uygur G, Hanley L. 2012. Quantification of antibiotic in biofilm-inhibiting multilayers by 7.87 eV laser desorption postionization MS imaging. *Anal. Chem.* 84:9410–15
39. Heinbuch S, Grisham M, Martz D, Rocca JJ. 2005. Demonstration of a desk-top size high repetition rate soft X-ray laser. *Opt. Express* 13:4050–55
40. Dong F, Heinbuch S, Xie Y, Bernstein ER, Rocca JJ, et al. 2009. C=C bond cleavage on neutral $VO_3(V_2O_5)_n$ clusters. *J. Am. Chem. Soc.* 131:1057–66
41. Gasper GL, Takahashi LK, Zhou J, Ahmed M, Moore JF, Hanley L. 2011. Comparing vacuum and extreme ultraviolet radiation for postionization of laser desorbed neutrals from bacterial biofilms and organic fullerenes. *Nuclear Instrum. Methods Phys. Res. A* 649:222–24
42. Heimann PA, Koike M, Hsu CW, Blank D, Yang XM, et al. 1997. Performance of the vacuum ultraviolet high-resolution and high-flux beamline for chemical dynamics studies at the Advanced Light Source. *Rev. Sci. Instrum.* 68:1945–51
43. Li Y, Qi F. 2009. Recent applications of synchrotron VUV photoionization mass spectrometry: insight into combustion chemistry. *Acc. Chem. Res.* 43:68–78
44. Zhou J, Takahashi LK, Wilson KR, Leone SR, Ahmed M. 2010. Internal energies of ion-sputtered neutral tryptophan and thymine molecules determined by vacuum ultraviolet photoionization. *Anal. Chem.* 82:3905–13
45. Kostko O, Takahashi LK, Ahmed M. 2011. Desorption dynamics, internal energies and imaging of organic molecules from surfaces with laser desorption and vacuum ultraviolet (VUV) photoionization. *Chem. Asian J.* 6:3066–76
46. Hanna SJ, Campuzano-Jost P, Simpson EA, Robb DB, Burak I, et al. 2009. A new broadly tunable (7.4–10.2 eV) laser based VUV light source and its first application to aerosol mass spectrometry. *Int. J. Mass Spectrom.* 279:134–46
47. Todt MA, Albert DR, Davis HF. 2016. High intensity vacuum ultraviolet and extreme ultraviolet production by noncollinear mixing in laser vaporized media. *Rev. Sci. Instrum.* 87:063106
48. Trevor JL, Mencer DE, Lykke KR, Pellin MJ, Hanley L. 1997. Surface mass spectrometry of biotinylated self-assembled monolayers. *Anal. Chem.* 69:4331–38
49. Levis RJ. 1994. Laser desorption and ejection of biomolecules from the condensed phase into the gas phase. *Annu. Rev. Phys. Chem.* 45:483–518
50. Dreisewerd K. 2003. The desorption process in MALDI. *Chem. Rev.* 103:395–425
51. Ready JF. 1971. *Effects of High-Power Laser Radiation*. New York: Academic

52. Land DP, Wang DTS, Tai T-L, Sherman MG, Hemminger JC, McIver RT Jr. 1990. Postionization of laser-desorbed neutrals for the analysis of molecular adsorbates on surfaces. In *Lasers and Mass Spectrometry*, ed. DM Lubman, pp. 157–78. New York: Oxford Univ. Press
53. Siegel MM, Tabei K, Tsao R, Pastel MJ, Pandey RK, et al. 1999. Comparative mass spectrometric analyses of photofrin oligomers by fast atom bombardment mass spectrometry, UV and IR matrix-assisted laser desorption/ionization mass spectrometry, electrospray ionization mass spectrometry, and laser desorption/jet-cooling photoionization mass spectrometry. *J. Mass Spectrom.* 34:661–69
54. Marksteiner M, Haslinger P, Sclafani M, Ulbricht H, Arndt M. 2009. UV and VUV ionization of organic molecules, clusters, and complexes. *J. Phys. Chem. A* 113:9952–57
55. Sezer U, Schmid P, Felix L, Mayor M, Arndt M. 2015. Stability of high-mass molecular libraries: the role of the oligoporphyrin core. *J. Mass Spectrom.* 50:235–39
56. Tatra S, Vázquez RG, Stiglbrunner C, Otto A. 2016. Numerical simulation of laser ablation with short and ultra-short pulses for metals and semiconductors. *Phys. Proc.* 83:1339–46
57. Yagnik GB, Hansen RL, Korte AR, Reichert MD, Vela J, Lee YJ. 2016. Large scale nanoparticle screening for small molecule analysis in laser desorption ionization mass spectrometry. *Anal. Chem.* 88:8926–30
58. Zinovev AV, Veryovkin IV, Moore JF, Pellin MJ. 2007. Laser-driven acoustic desorption of organic molecules from back-irradiated solid foils. *Anal. Chem.* 79:8232–41
59. Huang Z, Ossenbrüggen T, Rubinsky I, Schust M, Horke DA, Küpper J. 2018. Development and characterization of a laser-induced acoustic desorption source. *Anal. Chem.* 90:3920–27
60. Ellis SR, Soltwisch J, Paine MRL, Dreisewerd K, Heeren RMA. 2017. Laser post-ionisation combined with a high resolving power orbitrap mass spectrometer for enhanced MALDI-MS imaging of lipids. *Chem. Commun.* 53:7246–49
61. Deleted in proof
62. Pleticha FD, Lee D, Sinnott SB, Bolotin IL, Majeski MW, Hanley L. 2012. Acetylene ion-enhanced bonding of PbS nanoparticles to quaterthiophene in thin films. *J. Phys. Chem. C* 116:21693–98
63. Pan Y, Yin H, Zhang T, Guo H, Sheng L, Qi F. 2008. The characterization of selected drugs with infrared laser desorption/tunable synchrotron vacuum ultraviolet photoionization mass spectrometry. *Rapid Commun. Mass Spectrom.* 22:2515–20
64. Pomerantz AE, Hammond MR, Morrow AL, Mullins OC, Zare RN. 2008. Two-step laser mass spectrometry of asphaltenes. *J. Am. Chem. Soc.* 130:7216–17
65. Sabbah H, Morrow AL, Pomerantz AE, Zare RN. 2011. Evidence for island structures as the dominant architecture of asphaltenes. *Energy Fuels* 25:1597–604
66. Wang W, Taylor C, Hu H, Humphries KL, Jaini A, et al. 2017. Nanoaggregates of diverse asphaltenes by mass spectrometry and molecular dynamics. *Energy Fuels* 31:9140–51
67. Yang Q, Hu Y, Wei Y, Wang H, Guan J, et al. 2013. In situ detection of methylene blue in tissues by laser desorption vacuum ultraviolet single photon postionization mass spectrometry. *Int. J. Mass Spectrom.* 353:12–18
68. Lu Q, Hu Y, Chen J, Jin S. 2017. Laser desorption postionization mass spectrometry imaging of folic acid molecules in tumor tissue. *Anal. Chem.* 89:8238–43
69. Liu R, Yin Z, Cheng X, Meng Y, Hang W, Huang B. 2018. Confirmatory surface analysis of equivocal documents with pigment-based gel inks via laser desorption laser postionization mass spectrometry imaging. *Anal. Bioanal. Chem.* 410:1445–52
70. Fichou D, ed. 1999. *Handbook of Oligo- and Polythiophenes*. Weinheim, Ger.: Wiley-VCH
71. Hall-Stoodley L, Costerton JW, Stoodley P. 2004. Bacterial biofilms: from the natural environment to infectious diseases. *Nat. Rev. Microbiol.* 2:95–108
72. Kostakioti M, Hadjifrangiskou M, Hultgren SJ. 2013. Bacterial biofilms: development, dispersal, and therapeutic strategies in the dawn of the postantibiotic era. *Cold Spring Harb. Perspect. Biol.* 3:a010306
73. Bhardwaj C, Cui Y, Hofstetter T, Liu SY, Bernstein HC, et al. 2013. Differentiation of microbial species and strains in coculture biofilms by multivariate analysis of laser desorption postionization mass spectra. *Analyst* 138:6844–51
74. Boesl U. 1991. Multiphoton excitation and mass-selective ion detection for neutral and ion spectroscopy. *J. Phys. Chem.* 95:2949–62

75. Boesl U. 2000. Laser mass spectrometry for environmental and industrial chemical trace analysis. *J. Mass Spectrom.* 35:289–304
76. Streibel T, Zimmermann R. 2014. Resonance-enhanced multiphoton ionization mass spectrometry (REMPI-MS): applications for process analysis. *Annu. Rev. Anal. Chem.* 7:361–81
77. Boesl U, Kartouzian A. 2016. Mass-selective chiral analysis. *Annu. Rev. Anal. Chem.* 9:343–64
78. Getty SA, Brinckerhoff WB, Cornish T, Ecelberger S, Floyd M. 2012. Compact two-step laser time-of-flight mass spectrometer for in situ analyses of aromatic organics on planetary missions. *Rapid Commun. Mass Spectrom.* 26:2786–90
79. Henderson BL, Gudipati MS. 2014. Plume composition and evolution in multicomponent ices using resonant two-step laser ablation and ionization mass spectrometry. *J. Phys. Chem. A* 118:5454–63
80. Strickland D, Mourou G. 1985. Compression of amplified chirped optical pulses. *Opt. Commun.* 56:219–21
81. Cui Y. 2015. *The application of ultrafast laser pulses to laser desorption mass spectrometry*. PhD Thesis, Univ. Ill., Chicago
82. Lockyer NP, Vickerman JC. 1998. Multiphoton ionization mass spectrometry of small biomolecules with nanosecond and femtosecond laser pulses. *Int. J. Mass Spectrom. Ion Process.* 176:77–86
83. Lockyer NP, Vickerman JC. 2000. Single photon and femtosecond multiphoton ionisation of the dipeptide valyl-valine. *Int. J. Mass Spectrom. Ion Process.* 197:197–209
84. Kouno H, Imasaka T. 2016. The efficiencies of resonant and nonresonant multiphoton ionization in the femtosecond region. *Analyst* 141:5274–80
85. Kucher A, Jackson LM, Lerach JO, Bloom AN, Popczun NJ, et al. 2014. Near infrared (NIR) strong field ionization and imaging of C_{60} sputtered molecules: overcoming matrix effects and improving sensitivity. *Anal. Chem.* 86:8613–20
86. Breuer L, Kucher A, Herder M, Wucher A, Winograd N. 2014. Formation of neutral In_mC_n clusters under C_{60} ion bombardment of indium. *J. Phys. Chem. A* 118:8542–52
87. Chen Z, Vertes A. 2008. Early plume expansion in atmospheric pressure midinfrared laser ablation of water-rich targets. *Phys. Rev. E* 77:036316
88. Nemes P, Barton AA, Vertes A. 2009. Three-dimensional imaging of metabolites in tissues under ambient conditions by laser ablation electrospray ionization mass spectrometry. *Anal. Chem.* 81:6668–75
89. Zou J, Wu C, Robertson WD, Zhigilei LV, Miller RJ. 2016. Molecular dynamics investigation of desorption and ion separation following picosecond infrared laser (PIRL) ablation of an ionic aqueous protein solution. *J. Chem. Phys.* 145:204202
90. Petersen H, Tavakoli F, Kruber S, Münscher A, Gliese A, et al. 2016. Comparative study of wound healing in rat skin following incision with a novel picosecond infrared laser (PIRL) and different surgical modalities. *Lasers Surg. Med.* 48:385–91
91. Lu Y, Pieterse CL, Robertson WD, Miller RJD. 2018. Soft picosecond infrared laser extraction of highly charged proteins and peptides from bulk liquid water for mass spectrometry. *Anal. Chem.* 90:4422–28
92. Russo RE, Mao X, Mao SS. 2002. The physics of laser ablation in microchemical analysis. *Anal. Chem.* 74:70A–77A
93. Vogel A, Venugopalan V. 2003. Mechanisms of pulsed laser ablation of biological tissues. *Chem. Rev.* 103:577–644
94. Gattass RF, Mazur E. 2008. Femtosecond laser micromaching in transparent materials. *Nat. Photon.* 2:219–25
95. Vogel A, Noack J, Huttman G, Paltauf G. 2005. Mechanisms of femtosecond laser nanosurgery of cells and tissues. *Appl. Phys. B* 81:1015–45
96. Masuhara H. 2013. Time-resolved spectroscopic and imaging studies on laser ablation of molecular systems: from mechanistic study to bio/nano applications. *Bull. Chem. Soc. Jpn.* 86:755–83
97. Maxwell S, Mazur E. 2005. Nanoprocessing of subcellular targets using femtosecond laser pulses. *Med. Laser Appl.* 20:193–200
98. Liu Y, Sun S, Singha S, Cho MR, Gordon RJ. 2005. 3D femtosecond laser patterning of collagen for directed cell attachment. *Biomaterials* 26:4597–605

99. Cui Y, Moore JF, Milasinovic S, Liu Y, Gordon RJ, Hanley L. 2012. Depth profiling and imaging capabilities of an ultrashort pulse laser ablation time of flight mass spectrometer. *Rev. Sci. Instrum.* 83:093702
100. Milasinovic S, Cui Y, Gordon RJ, Hanley L. 2014. Internal energy of thermometer ions formed by femtosecond laser desorption: implications for mass spectrometric imaging. *J. Phys. Chem. C* 118:28938–47
101. Milasinovic S, Liu Y, Bhardwaj C, Blaze MTM, Gordon RJ, Hanley L. 2012. Feasibility of depth profiling of animal tissue by ultrashort pulse laser ablation. *Anal. Chem.* 84:3945–51
102. Milasinovic S, Liu Y, Gasper GL, Zhao Y, Johnston JL, et al. 2010. Ultrashort pulse laser ablation for depth profiling of bacterial biofilms. *J. Vac. Sci. Technol. A* 28:647–51
103. Zhang B, He M, Hang W, Huang B. 2013. Minimizing matrix effect by femtosecond laser ablation and ionization in elemental determination. *Anal. Chem.* 85:4507–11
104. Moreno-García P, Grimaudo V, Riedo A, Tulej M, Wurz P, Broekmann P. 2016. Towards matrix-free femtosecond-laser desorption mass spectrometry for *in situ* space research. *Rapid Commun. Mass Spectrom.* 30:1031–36
105. Grimaudo V, Moreno-García P, Riedo A, Meyer S, Tulej M, et al. 2017. Toward three-dimensional chemical imaging of ternary Cu–Sn–Pb alloys using femtosecond laser ablation/ionization mass spectrometry. *Anal. Chem.* 89:1632–41
106. Grimaudo V, Moreno-García P, Riedo A, Neuland MB, Tulej M, et al. 2015. High-resolution chemical depth profiling of solid material using a miniature laser ablation/ionization mass spectrometer. *Anal. Chem.* 87:2037–41
107. Neuland MB, Grimaudo V, Mezger K, Moreno-García P, Riedo A, et al. 2016. Quantitative measurement of the chemical composition of geological standards with a miniature laser ablation/ionization mass spectrometer designed for in situ application in space research. *Meas. Sci. Technol.* 27:035904
108. Griffiths RL, Sarsby J, Guggenheim EJ, Race AM, Steven RT, et al. 2013. Formal lithium fixation improves direct analysis of lipids in tissue by mass spectrometry. *Anal. Chem.* 85:7146–53
109. Walker AV, Gelb LD, Barry GE, Subanajouy P, Poudel A, et al. 2018. Femtosecond laser desorption ionization mass spectrometry imaging and multivariate analysis of lipids in pancreatic tissue. *Biointerphases* 13:03B416
110. Kuznetsov I, Filevich J, Dong F, Woolston M, Chao W, et al. 2015. Three-dimensional nanoscale molecular imaging by extreme ultraviolet laser ablation mass spectrometry. *Nat. Commun.* 6:6944
111. Wang J, Liu F, Mo Y, Wang Z, Zhang S, Zhang X. 2017. A new instrument of VUV laser desorption/ionization mass spectrometry imaging with micrometer spatial resolution and low level of molecular fragmentation. *Rev. Sci. Instrum.* 88:114102
112. Wang J, Wang Z, Liu F, Cai L, Pan J-B, et al. 2018. Vacuum ultraviolet laser desorption/ionization mass spectrometry imaging of single cells with submicron craters. *Anal. Chem.* 90:10009–15
113. Müller R, Kuznetsov I, Arbelo Y, Trottmann M, Menoni CS, et al. 2018. Depth-profiling microanalysis of CoNCN water-oxidation catalyst using a $\lambda = 46.9$ nm plasma laser for nano-ionization mass spectrometry. *Anal. Chem.* 90:9234–40
114. Vekey K. 1996. Internal energy effects in mass spectrometry. *J. Mass Spectrom.* 31:445–63
115. Luo G, Marginean I, Vertes A. 2002. Internal energy of ions generated by matrix-assisted laser desorption/ionization. *Anal. Chem.* 74:6185–90
116. Gabelica V, Schulz E, Karas M. 2004. Internal energy build-up in matrix-assisted laser desorption/ionization. *J. Mass Spectrom.* 39:579–93
117. Kostko O, Bandyopadhyay B, Ahmed M. 2016. Vacuum ultraviolet photoionization of complex chemical systems. *Annu. Rev. Phys. Chem.* 67:19–40
118. Niehaus M, Soltwisch J. 2018. New insights into mechanisms of material ejection in MALDI mass spectrometry for a wide range of spot sizes. *Sci. Rep.* 8:7755
119. Trimpin S. 2016. "Magic" ionization mass spectrometry. *J. Am. Soc. Mass Spectrom.* 27:4–21
120. Schneider BB, Lock C, Covey TR. 2005. AP and vacuum MALDI on a QqLIT instrument. *J. Am. Soc. Mass Spectrom.* 16:176–82
121. Wu C, Dill AL, Eberlin LS, Cooks RG, Ifa DR. 2013. Mass spectrometry imaging under ambient conditions. *Mass Spectrom. Rev.* 32:218–43

122. Ehlert S, Hölzer J, Rittgen J, Pütz M, Schulte-Ladbeck R, Zimmermann R. 2013. Rapid on-site detection of explosives on surfaces by ambient pressure laser desorption and direct inlet single photon ionization or chemical ionization mass spectrometry. *Anal. Bioanal. Chem.* 405:6979–93
123. Flanigan PM, Shi F, Perez J, Karki S, Pfeiffer C, et al. 2014. Determination of internal energy distributions of laser electrospray mass spectrometry using thermometer ions and other biomolecules. *J. Am. Soc. Mass Spectrom.* 25:1572–82
124. Nemes P, Huang H, Vertes A. 2012. Internal energy deposition and ion fragmentation in atmospheric-pressure mid-infrared laser ablation electrospray ionization. *Phys. Chem. Chem. Phys.* 14:2501–7
125. Bhardwaj C, Hanley L. 2014. Ion sources for mass spectrometric identification and imaging of molecular species. *Nat. Prod. Rep.* 31:756–67
126. Vaikkinen A, Shrestha B, Kauppila TJ, Vertes A, Kostiainen R. 2012. Infrared laser ablation atmospheric pressure photoionization mass spectrometry. *Anal. Chem.* 84:1630–36
127. Wu Q, Zare RN. 2015. Laser desorption lamp ionization source for ion trap mass spectrometry. *J. Mass Spectrom.* 50:160–64
128. Benham K, Hodyss R, Fernández FM, Orlando TM. 2016. Laser-induced acoustic desorption atmospheric pressure photoionization via VUV-generating microplasmas. *J. Am. Soc. Mass Spectrom.* 27:1805–12
129. Yung YP, Wickramasinghe R, Vaikkinen A, Kauppila TJ, Veryovkin IV, Hanley L. 2017. Solid sampling with a diode laser for portable ambient mass spectrometry. *Anal. Chem.* 89:7297–301
130. Laiko VV, Moyer SC, Cotter RJ. 2000. Atmospheric pressure MALDI/ion trap mass spectrometry. *Anal. Chem.* 72:5239–43
131. Kompauer M, Heiles S, Spengler B. 2016. Atmospheric pressure MALDI mass spectrometry imaging of tissues and cells at 1.4-μm lateral resolution. *Nat. Methods* 14:90–96
132. Diologent L, Bolbach G, Focsa C, Ziskind M, Fournier I. 2017. Laser induced post-desolvation of MALDI clusters. *Int. J. Mass Spectrom.* 416:29–36
133. Shi F, Flanigan PM, Archer JJ, Levis RJ. 2015. Ambient molecular analysis of biological tissue using low-energy, femtosecond laser vaporization and nanospray postionization mass spectrometry. *J. Am. Soc. Mass Spectrom.* 27:542–51
134. Isinger M, Squibb RJ, Busto D, Zhong S, Harth A, et al. 2017. Photoionization in the time and frequency domain. *Science* 358:893–96